



# Stability of Gate Roads Next to an Irregular Yield Pillar: A Case Study

Guorui Feng<sup>1</sup> · Pengfei Wang<sup>1</sup> · Yoginder P. Chugh<sup>2,3</sup>

Received: 26 January 2018 / Accepted: 16 June 2018 / Published online: 3 July 2018  
© Springer-Verlag GmbH Austria, part of Springer Nature 2018

## Abstract

This paper presents results for using an irregular yield pillar for gate road stability in a split-level panel layout (SPL) at a coal mine. The mine extracts 8# and 9# coal seams with a mudstone interlayer. SPL is being used to improve caveability for top coal. The tailgate is driven along the floor of 9# coal seam while the headgate is driven along the roof of 8# coal seam producing a gradually elevated (or curved) section on one end of the panel. Therefore, the gate pillar is of irregular shape and consists of two coal seams and a sandwiched mudstone interlayer. The stability of the tailgate next to this type of irregular yield pillar was investigated using numerical modelling and validated through field measurements and observations. The results show that tailgate with a 6-m-wide pillar has the minimum deformation. The sandwiched mudstone interlayer increases overall stability of tailgate and the yield pillar. The yield zone is smaller especially for the roof of the tailgate which provides a better support condition for the tailgate. Roof-to-floor convergence is smaller than rib-to-rib convergence. The intact zone in the curved section contributes to the overall stability of the gate pillar. Field observations show that stability of the tailgate next to the 6-m SPL yield pillar was maintained along with reduction of other ground control problems.

**Keywords** Yield pillar · Interlayer · Tailgate stability · Numerical modeling

## List of symbols

$\sigma$	Stress applied to the gob materials (MPa)
$\sigma_c$	Compressive strength of the rock pieces
$\varepsilon$	Change in volume/original volume stress (m/m),
$\varepsilon_m$	Maximum volumetric strain (m/m)
$E_0$	Initial tangential modulus (MPa)
$b$	Bulking factor
$H_c$	Height of caved zone (m)
$m$	Mining height (m)

## 1 Introduction

Gate road pillar or chain pillar plays a significant role in safe and efficient production in longwall mining. Pillars are required to provide adequate support capacity to maintain the stability of gate roads. However, there is a need to reduce

pillar width to maximize coal extraction and minimize roadway development (Seedsman et al. 2005).

Longwall top coal caving is extensively used in China. A longwall face experiences bulking-controlled caving. The caved roof strata becomes loose rock fragments which are subsequently compressed under the overburden pressure. The consolidation of the caved gob tends to reduce the pressure on the chain pillars between panels because a portion of the vertical load is assumed by the gob (Brady and Brown 2006). Caving of roof strata generally occurs after a large overhang which results in development of high mining-induced stresses and dynamic loading on supports (both, natural and applied) during caving (Gao et al. 2015; Bai et al. 2014; Singh et al. 2011). The overburden pressure above the opening, previously carried by the coal, is transferred from immediate roof to surrounding pillars. The stress redistribution depends upon the geological conditions, the mechanical properties of the rocks, the state of the in situ stresses, the layout of the panels, the mining sequence, etc. (Shabani-mashcool and Li 2013; Zhang et al. 2016). An increase in the width of the opening, generally, increases the value of the mining-induced stress and its range of influence over the surrounding pillars till caving occurs.

Pillar design is the primary engineering control for minimizing the risks of pillar failure and coal bursts in longwall

✉ Pengfei Wang  
18801448768@163.com

<sup>1</sup> College of Mining Engineering, Taiyuan University of Technology, Taiyuan 030024, China

<sup>2</sup> Department of Mining and Mineral Resources, Southern Illinois University, Carbondale, IL 62901, USA

<sup>3</sup> National Academy of Inventors, Tampa, FL, USA

mining. Stability and load bearing characteristics of the pillar depend on several factors including mechanical properties of the roof strata, cover depth, panel geometry, etc. Many studies (Li et al. 2015; Shen 2014; Yu et al. 2016; Zhang et al. 2017; Cao et al. 2016; Han et al. 2016; Chen et al. 2017) indicate that the coal pillar plays a key role in roadway stability. Mining engineers endeavor to avoid “critical” pillars which are too large to yield non-violently or too small to support large abutment loads (Agapito 1997; Mark 2016).

Several researchers proposed gob-side entry and yield pillar design approaches for ground control (Yan et al. 2013; Tan et al. 2015; Li et al. 2016a, b; Wang et al. 2017a, b). Due to the effect of moving of front abutment pressure with the advance of an active panel, the yield pillar along the gob is subjected to a complex dynamic loading during their service life. Therefore, determining optimum width of the pillar is a challenge (Shabanimashcool and Li 2012). Supplementary supports such as ladder beam, counter-pulled bolts and variations of pipe umbrella systems must be used for ground control that can result in higher production cost (define these support systems).

Wilson (1972) proposed a model for pillar strength that involved the width-to-height ratio and more complex modes of behavior with non-homogeneous stress levels within the pillar. DeMarco et al. (1995) indicated that the width-to-height ratios of burst-prone, critical pillars normally exceeded 4 or 5. In light of the significance of the width-to-height ratio of pillars, many researchers have studied the uniaxial compressive strength of coal for pillar design and determined how the values change with specimen size (Hustrulid 1976; Medhurst and Brown 1998). Seedsman (2005) concluded that the strength increases as the pillar height decreases and the rate of increase in strength is greater for width to height ratios in excess of 8:1. He also raised the questions: what is the height of a chain pillar when the longwall extraction height is greater than the development height? Is the location of the gate road a factor? He reported that most Australian longwalls have had the gate roads located along the floor of the seam which intuitively appears to be a less stable arrangement.

Barron (1984) observed that confinement around the pillar core and failure types were linked: low confinements produced brittle failures, and high confinements produced ductile failures. Madden (1991) reassessed the equation developed by Salamon and Munro (1967) in light of its past performance and examined the effect of mining method on coal pillar strength. Gale (1998) pointed out that the pillar strength and deformation of the adjacent roadways is a function of failure in the coal and the strata about the coal. In other word, the strength characteristics of pillars are dependent on the strength properties of the strata surrounding the coal, as well as on the properties on the coal pillar. He stated

that rather than the coal only, failure also occurs within the strata, and different strata-coal combinations (or strata-coal interaction) lead to the wide range of pillar strength characteristics. This may agree with the statement that the pillar strength is highly dependent on site-specific conditions (Yu et al. 2016). Colwell (1998) proposed ALTS which relates the increase in pillar load to the dead weight of a wedge of rock located over the side of the gob (defined by abutment angle model). Seedsman (2005) presented pillar design for mining practitioners employing limit-equilibrium type approaches that are readily accessible at mine sites. Ghasemi and Shahriar (2012) proposed a step-by-step method to design pillars with a square shape in room-and-pillar mines with regard to existing pillars in an active mining zone and estimated abutment loads using experimental equations. Recio-Gordo and Jimenez (2012) presented a novel method for probabilistic prediction of coal pillar performance using the analysis of longwall pillar stability (ALPS) and analysis of retreat mining pillar stability (ARMPS) methods for empirical pillar design of (respectively) longwall and retreat room-and-pillar operations.

However, coal pillar stability is strongly influenced by the site-specific geological and geotechnical conditions. Therefore, coal pillar design relying on such empirical approaches have significant shortcomings by taking only very few factors into account and ignoring site-specific conditions (Brady and Brown 2006; Maleki 2017). Oversimplification would bring about uncertainties in the results (Shabanimashcool and Li 2013). For instance, empirical subsidence prediction methods have not usually taken into account material behavior. Therefore, their results could be hardly extrapolated from one coal mining area to another, and even sometimes from panel to panel (Alejano et al. 1999).

Numerical modelling can include many more relevant factors in the analysis and allow for consideration of complex boundary conditions and material behavior so that the results may be more realistic (Mortazavi et al. 2009; Shabanimashcool and Li 2013). Numerical modelling validated through field measurements can achieve reliable results and this validation-based numerical modelling back analysis can also be used for future design. (Mark et al. 2007; Yan et al. 2013; Li et al. 2015). A large number of numerical modelling experiments on pillars have been conducted. Wang et al. (2013) numerically investigated dynamic mechanical state of a coal pillar during longwall mining panel extraction. Yasitli and Unver (2005) carried out numerical modeling of longwall mining with top-coal caving at M3 longwall panel at the Omerler underground mine. Mohan et al. (2001) presented a numerical estimation of pillar strength in coal mines. Shabanimashcool and Li (2012) carried out numerical modeling of longwall mining and stability analysis of the gates at Svea Nord coal mine in Svalbard. Using a numerical modeling code, 2-D rock failure process analysis, the progressive

failure process and associated acoustic emission behavior of serial and parallel rock samples were simulated by Wang et al. (2011).

However, the pillars studied in above research are generally rectangular or square. This paper presents an irregular pillar (non-rectangular and non-square) in a yield pillar application for gate road stability accompanied with a novel longwall mining layout to create a better cavability for top coal. Numerical modelling was used to study the stability of the gate road next to this type of irregular yield pillar. Field measurements were carried out to validate the numerical modelling and to investigate the deformation situation of the gate road and stress distribution within the yield pillar.

## 2 Background

A coal mine located on the west of Taiyuan City, the capital of Shanxi Province, North China was used for case study. 8# and 9# coal seams at the mine are mined at depth of around 340 m using longwall top coal caving mining method. The average output of the mine is 5 million tons per year. The stratigraphy at the mine generally consists of horizontally laminated or bedded sedimentary rocks comprised mostly of sandstone, mudstone and limestone with significantly contrasting mechanical properties as shown in Fig. 1. 8# and 9# coal seams average about 3.3 and 3.4 m in thickness, respectively. Average inclination of the coal seams is 8°. The 9# coal seam is underlain by carbonaceous mudstone (0.4 m) and sandy mudstone (11.9 m) in descending order. The 8# coal seam is overlain by mudstone (1.2 m), 8# upper coal seam (0.6 m) and limestone (3.0 m) in ascending order. There is a stratified mudstone interlayer between the two coal seams with an average thickness of 0.8 m. The density of the mudstone interlayer is 2600 kg/m<sup>3</sup>, uniaxial compressive strength is 2.9–9.8 MPa, tensile strength is 0.6–2.9 MPa, elastic modulus is 6.12 GPa.

A single entry longwall top coal caving retreat system which is commonly used in China is adopted at the coal mine. In this single entry retreat longwall mining, two gate roads are driven between 200 m apart. When the gate roads have been driven a predetermined length, 1400 m long, they are connected and a longwall block is outlined as shown in Fig. 2a. The longwall face is then installed at the setup room with top coal caving roof supports, shearer, front and rear armoured face conveyors (AFC), etc., throughout the whole width of the panel, the longwall face starts to advance towards the mains and it stops at the stopping line leaving a barrier pillar unmined to protect mains. As the shearer cuts the coal back and forth web by web all the way between the tailgate and the headgate, the rock bolts installed in the panel side ribs of the gate roads are fiberglass reinforced rock bolts that can be cut directly by shearer. The gate roads

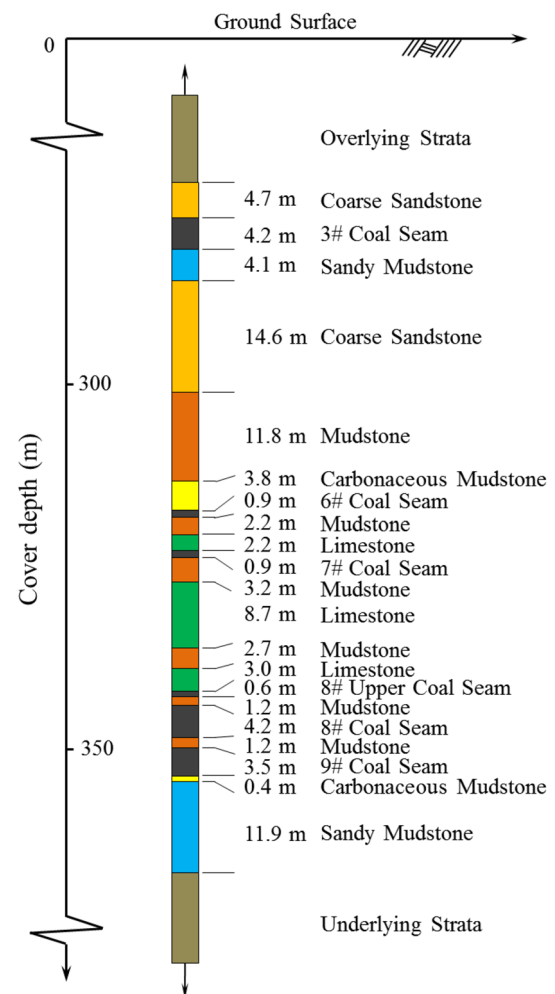
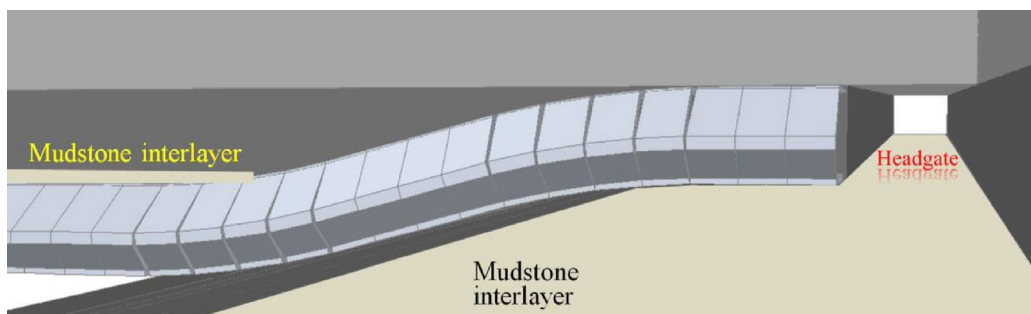
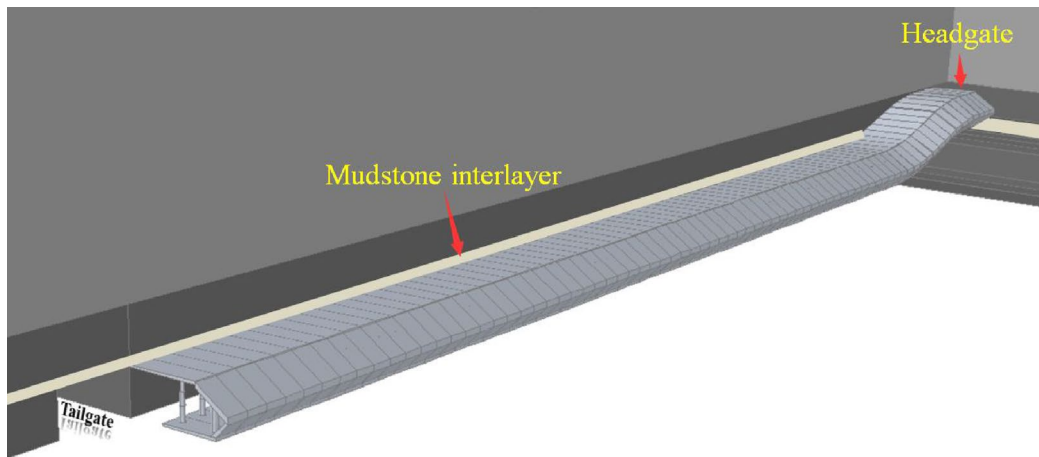
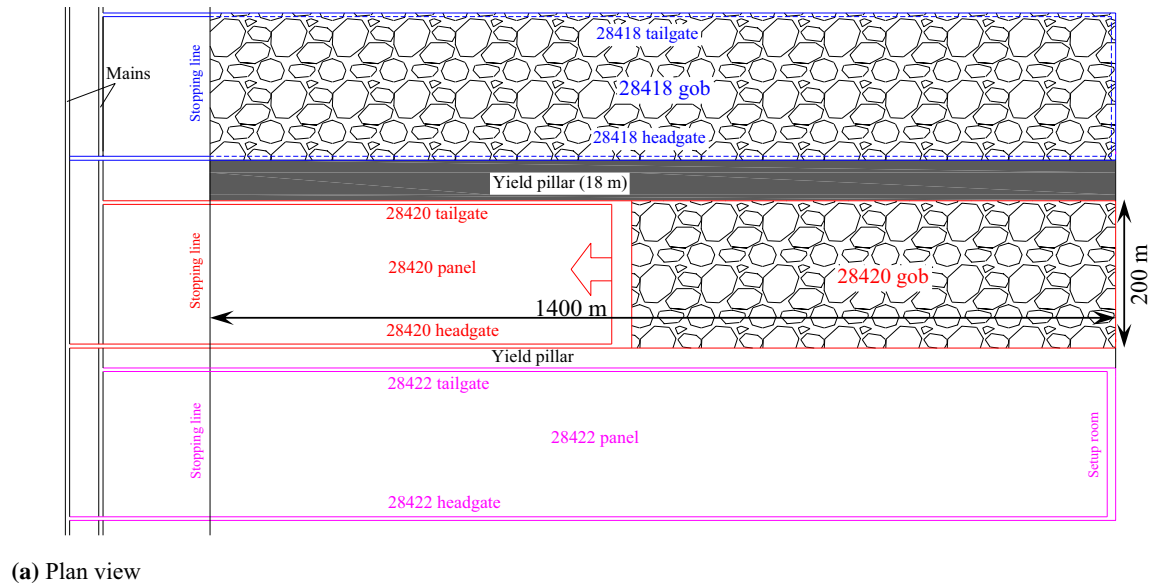


Fig. 1 Generalized stratigraphy column

are allowed to collapse behind the face line to form part of the gob. The gate roads are known as headgate and tailgate. The headgate contains the belt conveyor and the pantech-nicon for facilitating power and logistics to the longwall face.

There are two wings at the mine, that is why the panel numbers in one wing are all even numbers and the panel numbers in the other wing are all odd numbers. The tailgate entry development for the new panel should be done at least 300 m behind the working face of previous panel to avoid the dynamic mining induced influence. Two-wing system provides plenty of time for the roof strata of the mined panel to settle and their movement cease before a new tailgate entry development. For instance, when a panel in the left wing is being extracted, the entry in the right wing can be excavated for preparing a new panel. Thus, the dynamic loading due to mining-induced influence is avoided during the entry development.

The mudstone interlayer does not have a significant influence on top coal caving and flowing using the split-level



**Fig. 2** Split-level panel layout (SPL) at the case study coal mine

panel layout (SPL) or longwall mining with split-level gate roads (LMSG) as shown in Fig. 2b, c (Wang et al. 2017a, b; Zhao et al. 2017). Gate roads on either end of a SPL panel are located at different elevations within the 8# and 9# coal seams. The tailgate is driven along the floor of 9# coal seam

while the headgate is driven along the roof of 8# coal seam. Thus, the mining geometry consists of a gradually elevated section on the right end of the panel. By employing SPL, the mudstone interlayer and 8# coal seam were pre-cut through creating free surfaces for the two parts of the interlayer

as shown in Fig. 2b, c. Therefore, when the working face advances in the in-plane direction, mudstone interlayer caves better so that fragmentation of mudstone blocks does not cause difficulty in top coal caving, flowing or drawing. The mudstone interlayer averages about 0.8 m. But its thickness varies from locations to locations. For locations where mudstone interlayer is thick, say more than 1.2 m, the sizes of the mudstone blocks maybe very big. Big blocks do harm to rear canopies and AFC, so experienced miners close the rear canopies immediately as soon as they hear the big blocks flowing towards the rear canopies. For medium size mudstone pieces which are easily distinguished and picked out (which depends on the colors of the constituent of the mudstone, it also varies from locations to locations), miners separate them out underground and deposit them in mined-out areas. For some locations where mudstone interlayer is thin, say less than 0.4 m, then the small mudstone fragmentations are directly transported to the processing plant and are separated manually and mechanically there.

Before employing SPL, the coal mine used the conventional panel layout, that is, the gate roads were all driven along the floor, the rectangular gate pillar (18 m wide) was left unmined between adjacent panels. This layout led to several problems for this coal mine case. First, the mudstone interlayer had a significant influence on cavability of top coal due to the inability of the interlayer to cave without delay and large fragmentation of caved mudstone rocks. Previous mining practices show that the large caved mudstone rocks were frequently stuck at the sliding rear canopies when it was open to allow top coal to fall through onto the rear AFC which prevented the top coal above the interlayer from flowing and thus reduced the recovery rate significantly. Second, the 18 m wide gate pillar led to difficulty in gate road stability such as rib sloughing, breaking of rock bolts, and roof convergence. The maximum roof-to-floor and rib-to-rib convergences of 28,420 tailgate during the development of the entry were 375 and 429 mm, respectively, while that during the extraction of the panel were 1452 and 1527 mm,

respectively. Investigation conducted last year showed that this was due to stress concentration on the gate pillar. Coal bursts occurred several times that led to lost production for weeks and months. To mitigate burst risk, 6 m SPL yield pillar was employed between 28,420 and 28,422 panel. All gate roads are rectangular, 4.6 m wide and 3 m high, respectively. Rock bolts and cable bolts are used for gate road support. As the rib-to-rib convergences are large, the cable bolts are used for rib convergence control as shown in Fig. 3. The rock bolts are 2.4 m long and cable bolts are 4 m long. Advanced support was employed for the gate road with a range of 0–50 m ahead of the working face which will be presented in detail in later section.

### 3 Numerical Modelling

The SPL gate pillar shown in Fig. 4 is of irregular shape and consists of two coal seams and a mudstone interlayer, theoretical or empirical analysis is very difficult to implement and results may not be applicable. Therefore, numerical modelling validated by field measurements was carried out to study the stability of the gate road next to this irregular yield pillar.

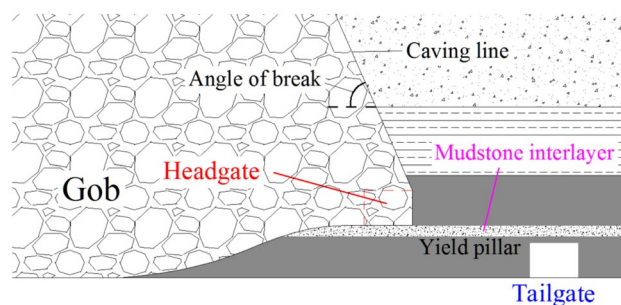
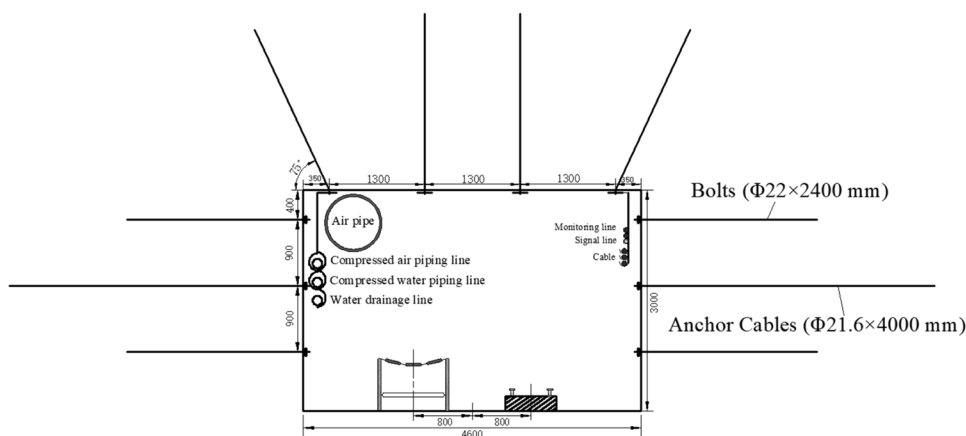


Fig. 4 SPL gate pillar with an irregular shape and mudstone interlayer

Fig. 3 Support pattern for gate roads





### 3.1 The Overall Model Geometry and Simulation Plans

As stated earlier, the yield pillar between 28,420 and 28,422 SPL panel is irregular, i.e., the shape is neither rectangular nor square, the pillar consists not only of coal, but with a thin mudstone interlayer sandwiched between the two super-adjacent coal seams. Therefore, numerical modelling employing FLAC<sup>3D</sup> code was carried out to study the stability of the gate road next to this composite and unconventional gate pillar.

The developed FLAC<sup>3D</sup> model (Corkum and Board 2016) is shown in Fig. 5. One-half of each of 28,420 and 28,422 panels and the gate roads system were incorporated in the model considering the symmetry. The dimension of the model was 200 m (length) × 10 m (width) × 120 m (height). A uniform stress of  $250 \text{ m} \times 0.025 \text{ MN/m}^3 = 6.25 \text{ MPa}$  was applied to the top of the model corresponding to 250 m of overburden strata by assuming the overlying unit weight was  $0.025 \text{ MN/m}^3$ . A significant distance to the lateral boundaries and the bottom boundary was used to minimize model

boundary effects. The mesh size graded from small, around material boundaries, to large at the center of a material domain. Fine zone resolution in the vicinity of gate roads, gate pillar, coal seam unit and gob was generated for accurate prediction of progressive yielding and deformation. The side boundaries were roller constrained and the bottom boundary was fixed both horizontally and vertically. Using the small diameter borehole hydraulic fracturing stress measurement equipment (Kang et al. 2010), in situ stress measurements were conducted, the results supplemented by published data (Kang et al. 2010) are given in Table 1.

According to the in situ stress measurements results, an approximate ratio of horizontal to vertical stresses ( $K$ ) of 0.8 both along and across the panels was used. As the irregular composite gate pillar consists of two coal seams and a mudstone interlayer, interface plays a significant role in its failure process. Therefore, discontinuous model interfaces, representing bedding planes, capable of yielding and separating, were built into the model at the contact of each unit using FLAC interface logic (Wang et al. 2017a, b). Bolts were simulated by built-in cable structure element in

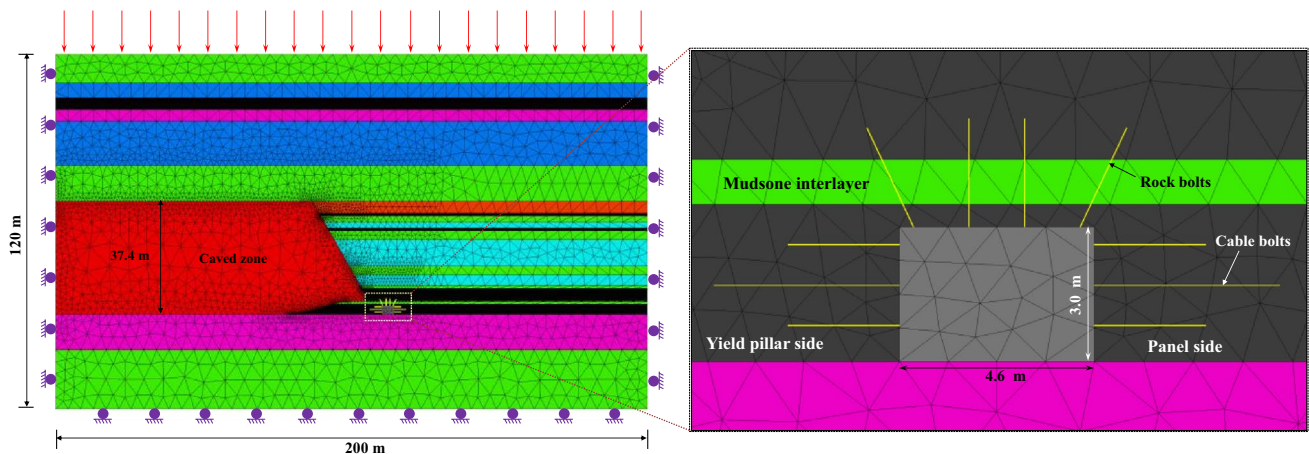


Fig. 5 FLAC<sup>3D</sup> model used for simulation

Table 1 Results of in situ stress measurements at the coal mine

No.	Depth	Vertical principal stress, $\sigma_v$ (MPa)	Maximum horizontal principal stress, $\sigma_H$ (MPa)	Minimum horizontal principal stress, $\sigma_h$ (MPa)	Orientation of maximum horizontal principal stress, $\sigma_H$ (MPa)
1	636	15.90	13.16	6.75	N73.6°W
2	622	15.55	13.99	7.17	N33.3°W
3	346	8.65	7.77	4.15	N89.7°W
4	379	9.48	7.57	4.01	N62.1°W
5	323	8.08	5.04	3.24	N86.2°W
6	325	8.13	6.36	3.47	N56.4°W
7	384	9.60	9.92	5.17	N58.1°W
8	403	10.08	10.92	5.23	N66.5°W

**Table 2** Mechanical and geometric parameters of support cable structure elements

Type	$E$ (GPa)	$C_g$ (N/m)	$K_g$ (N/m <sup>2</sup> )	$\rho_g$ (m)	$A$ (m <sup>2</sup> )	$F_t$ (N)
Rock bolt	200	4.7e5	5.6e9	8.79e−2	3.14e−4	1.6e5
Cable bolts	195	4.7e5	4.2e9	8.79e−2	2.49e−4	2.5e5

**Table 3** Properties of roof and floor strata for numerical modeling

Lithology	Height (m)	Depth (m)	Unit weight (kg/m <sup>3</sup> )	Cohesion (MPa)	Friction angle (°)	Compressive strength (MPa)	Bulk modulus (GPa)	Shear modulus (GPa)
Coarse sandstone	4.6	275.9	2700	5.52	41.3	24.42	18.9	14.2
3# coal seam	4.2	280.5	1400	1.35	29.2	4.59	11.9	7.1
Sandy mudstone	4.1	284.7	2600	2.51	34.9	9.63	13	8.5
Coarse sandstone	14.6	288.8	2700	5.52	41.3	24.42	18.9	14.2
Mudstone	11.8	303.4	2600	2.62	31.7	9.41	12.4	8.1
Carbonaceous mudstone	3.8	315.2	2500	1.35	29.2	4.59	11.9	7.1
6# coal seam	0.9	319.0	1400	1.35	29.2	4.59	11.9	7.1
Mudstone	2.2	319.9	2600	2.62	31.7	9.41	12.4	8.1
Limestone	2.2	322.1	2700	6.76	43.0	31.1	19.3	15.7
7# coal seam	0.9	324.3	1400	1.35	29.2	4.59	11.9	7.1
Mudstone	3.2	325.2	2600	2.62	31.7	9.41	12.4	8.1
Limestone	8.7	328.4	2700	6.76	43.0	31.1	19.3	15.7
Mudstone	2.7	337.1	2600	2.62	31.7	9.41	12.4	8.1
Limestone	3.5	339.8	2700	6.76	43.0	31.1	19.3	15.7
Mudstone	1.2	343.3	2600	2.62	31.7	9.41	12.4	8.1
8# coal seam	4.3	344.5	1400	1.35	29.2	4.59	11.9	7.1
Mudstone	1.2	348.8	2600	2.62	31.7	9.41	12.4	8.1
9# coal seam	3.5	350	1400	1.35	29.2	4.59	11.9	7.1
Sandy mudstone	11.9	353.5	2600	2.51	34.9	9.63	13	8.5

FLAC<sup>3D</sup> (Itasca 2007). Table 2 gives mechanical and geometric parameters for the cable structure elements (Zhang et al. 2014). Mohr–Coulomb constitutive model was used for the rock strata, strain-softening model (a cohesion and internal friction angle loss process) for the yield pillar and double-yield model for the gob which are to be defined later. Six yield pillar widths were simulated, i.e., 4, 6, 8, 10, 14 and 18 m.

### 3.2 Development of Parameters for Rock Strata and Yield Pillar

The properties of roof and floor strata were estimated through geotechnical testing of physico-mechanical properties of the freshly procured core samples using the suggested the International Society for Rock Mechanics (ISRM) standards. The results are presented in Table 3.

The progressive failure of coal pillar includes three phases, they are elastic phase, plastic softening phase and the residual phase. Jaiswal and Shrivastva (2009) noted that after yielding of the coal pillars, plastic softening occurs

**Table 4** Variation of mechanical properties of coal with plastic shear strain

Plastic strain	0	0.0025	0.005	0.0075	0.01
Cohesion (MPa)	0.8	0.68	0.54	0.40	0.28
Friction angle (°)	24	23	22	21	21

until a residual strength level is achieved. The most widely accepted model for coal pillars, Mohr–Coulomb strain-softening model assumes coal pillar as a nonlinear strain-softening material with cohesion and friction angle softening as a function of plastic strain. The post-peak properties of a strain-softening model are hard to estimate. In addition, the shape of yield pillar in this paper is irregular,  $W/H$  ratio cannot be simply used as a factor to calibrate the numerical models based on empirical methods or formula. Therefore, a trial-and-error method and past experience (Shen 2014) were used to determine the input properties to match stress distribution of the yield pillar with that obtained by field monitoring. The calibrated input properties for the strain-softening model are shown in Table 4.

### 3.3 Bedding Plane Interface Parameters

Coal/rock interface condition is very important to bump control (Meikle 1965; Khair 1968; Brauner 1994; Newman 2002; Peng 2008). It is true that pillar strength increases with increasing interface friction because the frictional constraint may create a confined state of stress in the pillar. Hence, to consider coal/rock interface strength in the numerical model, a direct shear test on the coal/rock interface was conducted. The test specimens were obtained from the drilled cores in the panel 28,420. The diameter and height of the specimens are 50 and 100 mm, respectively. The interface is located at mid-height of the specimen. After the test, the cohesion and friction angle of the coal/rock interface were determined to be 0.795 MPa and 31°, respectively. These two parameters will be used in the numerical model to simulate the coal/roof and coal/floor interfaces.

### 3.4 Gob Modelling

To date, there are three gob modelling methods. Jiang et al. (2012) and Wang et al. (2013) assumed the gob area to be a very soft elastic material to simulate the support capability of the fallen rock from the roof. Song et al. (2017) used estimated pre-set force against roof according to theoretical gob stress distribution to simulate the support capacity of the gob material employing Phase 2D software. Using the finite element package, ABAQUS and based on the Terzaghi's model, Morsy and Peng (2002) developed a numerical gob model. Esterhuizen et al. (2010) used equivalent gob elements that follow the hyperbolic stress–strain curves to model the gob compaction and response and carried out model calibration for simulation of coal pillars, gob and overburden response. Yavuz (2004), Li et al. (2015) Jiang et al. (2017) used Salamon's model to simulate the gob and obtained good results. However, the above studies did not take angles of break into account, and gobs are commonly filled by replacing the coal seam or coal seam and immediate roof. The generalized gob area is determined by field observation rather than only taking coal seam or coal seam and immediate roof as gob area. The field gob material at the face end behind the end shield is shown in Fig. 6.

Built-in double yield constitutive model in FLAC<sup>3D</sup> was used to simulate the gob in this study (Itasca 2007) and cap pressure for double yield model is estimated by Salamon's equation. Salamon's equation is expressed by:

$$\sigma = \frac{E_0 \varepsilon}{1 - (\varepsilon/\varepsilon_m)}, \quad (1)$$

where  $\sigma$  is the stress applied to the gob materials,  $\varepsilon$  is the volumetric strain under the applied stress,  $E_0$  is initial



Fig. 6 The cave rock material behind the end shield

tangential modulus and  $\varepsilon_m$  is maximum volumetric strain, and (Yavuz 2004):

$$E_0 = \frac{1.039\sigma_c^{1.042}}{b^{7.7}}, \quad (2)$$

$$\varepsilon_m = \frac{b-1}{b}, \quad (3)$$

where  $\sigma_c$  is the compressive strength of the rock pieces;  $b$  is the bulking factor, and (Peng 2006):

$$b = \frac{H_c + m}{H_c}, \quad (4)$$

where  $H_c$  is the height of caved zone and  $m$  is the mining height.

In addition, to be more realistic with the physical situation, angle of break (defined as the acute angle formed by the caving line and coal seam bedding plane) obtained from cross-measure boreholes and gob gas wells were incorporated in the numerical model. According to these boreholes and wells, the angle of break is about 65°; the height of the caved zone above the coal seam was about 28.5 m reaching 11.8 m thick mudstone. Hence, According to Eq. (1), the bulking factor, maximum strain and the initial modulus of the gob materials can be calculated as 1.31, 0.24 m/m and 44.4 MPa, respectively. Cap pressure for the double-yield model is given in Table 5 and is expressed by:

$$\sigma = \frac{44.36\varepsilon}{1 - 4.20\varepsilon}. \quad (5)$$

To obtain the parameters for gob and make sure that the stress–strain relationship agrees with Eq. (5), a simple model with dimensions 1 m (length) × 1 m (width) × 2 m (height)



**Table 5** Peak pressures for the double yield model

Strain (m/m)	Stress (MPa)	Strain (m/m)	Stress (MPa)
0.00	0.00	0.12	10.74
0.01	0.46	0.13	12.71
0.02	0.97	0.14	15.08
0.03	1.52	0.15	18.00
0.04	2.13	0.16	21.66
0.05	2.81	0.17	26.40
0.06	3.56	0.18	32.78
0.07	4.40	0.19	41.81
0.08	5.35	0.20	55.60
0.09	6.42	0.21	79.26
0.10	7.65	0.22	129.24
0.11	9.07	0.23	304.70

**Table 6** Parameters for gob material

Density (kg/m <sup>3</sup> )	Bulk modulus (GPa)	Shear modulus (GPa)	Friction (°)	Dilation (°)
1700	40	30	8.3	3

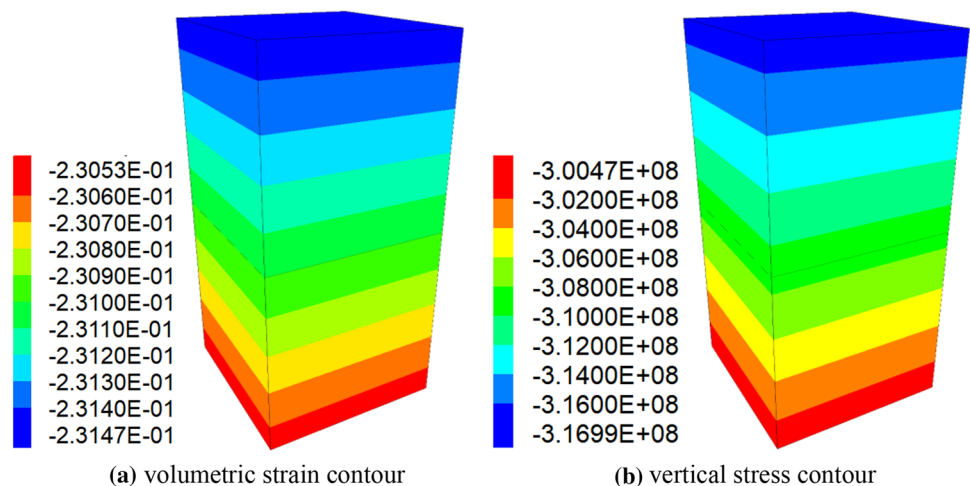
was built (to develop stress–strain behavior). Loading was simulated by applying a displacement velocity on the top surface with bottom surface fixed vertically and four side surfaces fixed horizontally. The input parameters were varied for the bulk and shear modulus, angle of dilation, angle of friction, and density of gob material. By trial and error, the final properties are given in Table 6. Figures 7 and 8 show the volumetric strain contour, vertical stress contour and comparison of simulated stress–strain curve with the Salamon’s model. They demonstrate that numerically obtained data agrees very well with Salamon’s equation. The modelling results before the excavation of the tailgate are shown in Fig. 9.

The higher elevation of the headgate of 28,420 panel moved the stress concentration zone with it. Therefore, the stress environment of tailgate of 28,422 panel was improved by locating all the gate road along the floor. The vertical stress increased from 0.086 MPa at the gob edge to 7.41 MPa at a distance of about 70 m from the gob edge and then remains relatively constant. In other words, 87.2% of the original vertical stress (7.41/8.5 MPa) is achieved within a distance of 20.6% of the panel overburden depth (70/340 m). King and Whittaker (1971) concluded that pre-mining stress is achieved at a distance of 0.6 times overburden depth. Based on an investigation and analysis of a large number of gate road stability cases, Wilson (1981) suggested that the vertical stress increases from zero to the original stress at a distance of 0.2–0.3 times overburden depth. Smart and Haley (1987) suggested that the reasonable estimate of cover stress distance should be 0.12 times overburden depth based on field measurement data. Mark (1990) indicated that the 0.38 times overburden depth is the cover stress distance. It can be seen that the stress distribution of the caved zone is in good agreement with other researchers’ conclusions. Therefore, the parameters calibrated through above steps can be used for gob modelling. Please note that the final set of inputs is not unique, and it is possible that a different combination of input values can equally satisfy the Salamon’s equation.

### 4 Modelling Results and Discussion

For 4 m yield pillar, the entire pillar was in a yield state. The support capacity of the pillar was almost completely lost sustaining only very low load with the maximum peak value of 5.4 MPa which is far less than pre-mining stress of 8.5 MPa. While the abutment load on the 28,422 panel side reaches 32.8 MPa. This indicates that 4 m yield pillar is crushed and fails to maintain the stability of 28,422 tailgate. Therefore,

**Fig. 7** The volumetric strain contour, vertical stress contour



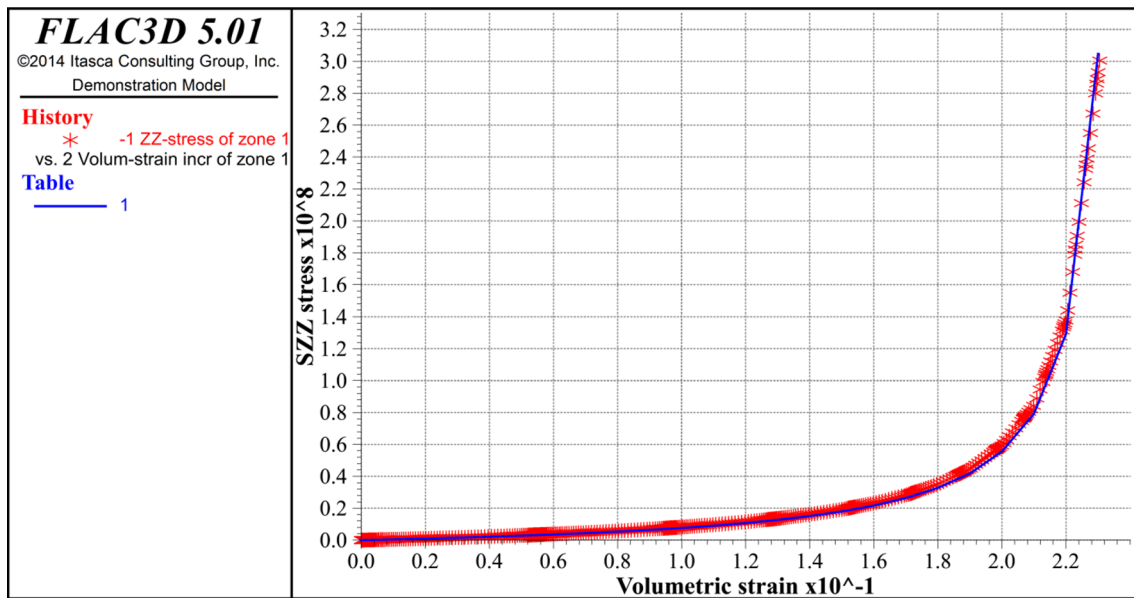


**Fig. 8** Comparison of simulated stress–strain curve with the salamon's model

4 m yield pillar should not be considered. What's more, the evident failure mode is shear failure (yellow elements) based on the angle of break. The depths of yielding on the yield pillar side and panel side are 6.8 and 5.5 m, respectively. Similar data for 8# coal seam is 8.8 m. The thin coal sheet between the mudstone interlayer and the tailgate is in shear and tension failure mode. However, the roof mudstone interlayer sandwiched between the two yielded parts of the two coal seams has not completely yielded above the 28,422 tailgate. Nearly half of the roof mudstone interlayer is intact although the coal above and beneath it is in yield state.

When the yield pillar width is increased from 4 to 6 m, the peak load increases dramatically from 5.4 to 12.2 MPa and the entire pillar in yield state. The peak abutment load on the 28,422 panel side decreases from 32.8 to 27.5 MPa. Most notably, the area of the yield zone on the 28,422 panel rib is much smaller than that in Fig. 10a. This suggests that the bearing capacity of the 6 m yield pillar increases significantly when the pillar size increases from 4 to 6 m.

For yield pillar with width of 8 or 10 m, the pillar is still in partially yield state. The peak abutment load on the yield pillar side increases from 17.6 MPa (8 m yield pillar) to 19.5 MPa (10 m yield pillar). While the peak abutment load on the 28,422 panel side decreases from 23.8 MPa (8 m yield pillar) to 22.7 MPa (10 m yield pillar). The area of the yield zone on the 28,422 panel rib in these two cases are similar to that in Fig. 10b and are also much smaller than that in Fig. 10a. This suggests that the bearing capacity of the yield pillar increases when the pillar size increases from 6 to 10 m.

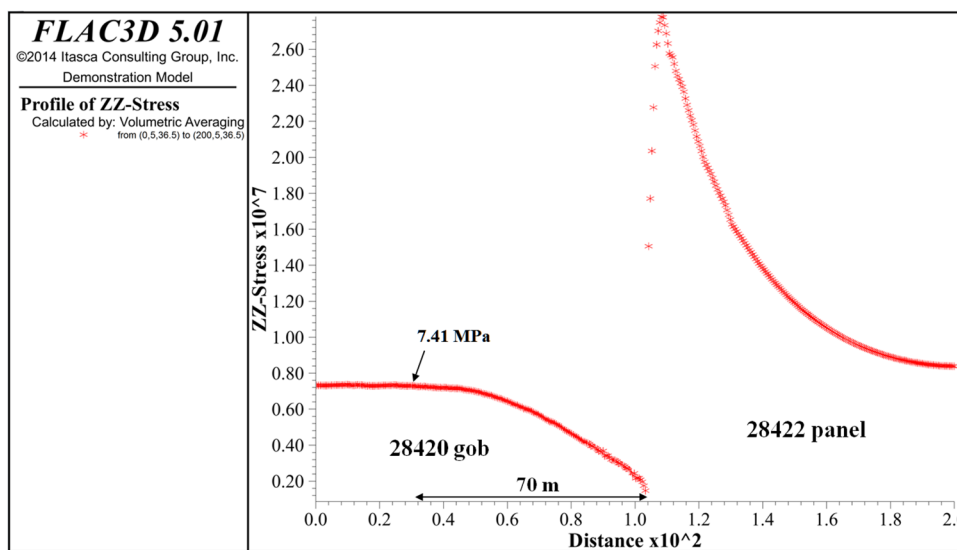
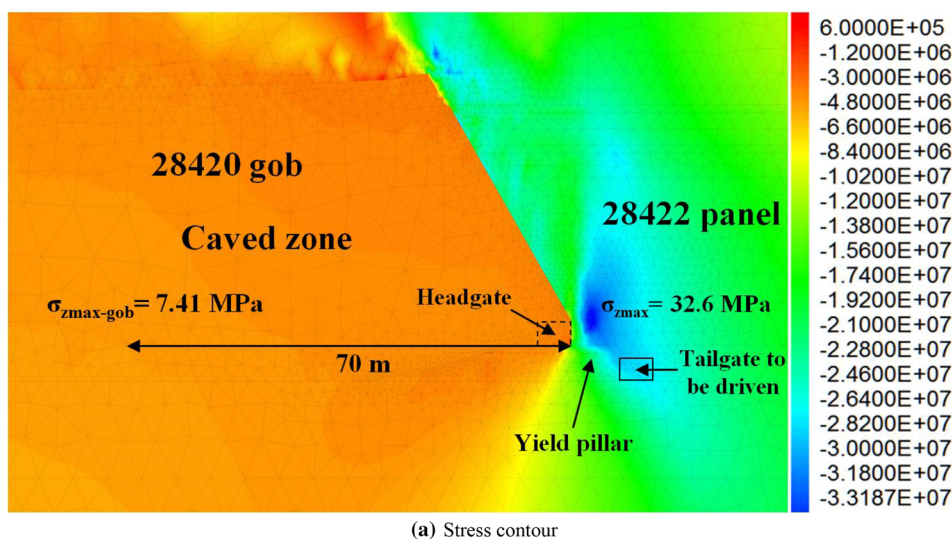
When the yield pillar is increased from 10 to 14 m, yield pillar peak pillar load increases sharply from 19.5 to

25.8 MPa, and become larger than the peak abutment on the panel side indicating that the ground pressure is mainly borne by the gate pillar. An intact zone is developed within the yield pillar when the coal pillar is 14 m. This may contribute to the sharp rise of the peak abutment load of the gate pillar. When the gate pillar is increased to 8 m, a double hump stress curve is developed. This is due to the increase of the size of the intact zone within the pillar.

Maximum rib-to-rib and roof-to-floor convergences were monitored and the layout for the 28,422 tailgate is shown in Fig. 11a. Differences of “AB” and “CD” with respect to their initial values represent rib-to-rib convergence and roof-to-floor convergence, respectively. The result is plotted in Fig. 11b. It shows that for all gate pillar sizes the roof-to-floor convergences are smaller than rib-to-rib convergences. The pillar width has more effect on rib convergence than roof–floor deformation. Tailgate with a 6-m-wide pillar has the minimum deformation under the current geological and geotechnical conditions.

The results shown in Figs. 10 and 11 clearly demonstrate that the load-bearing capacity of the yield pillar and gate road deformation vary with yield pillar widths and have a considerable effect on stability of the gate road. In addition, the mudstone interlayer has a significant influence on the overall stability of tailgate and the yield pillar. The yield zone development and connection of the 8# and 9# coal seams was cut off by this more competent interlayer, as a consequence, the yield zone is smaller especially for the roof of the tailgate. This provides a better support condition for the tailgate. This may explain

**Fig. 9** Modelling results before the excavation of the tailgate of 28,422 panel



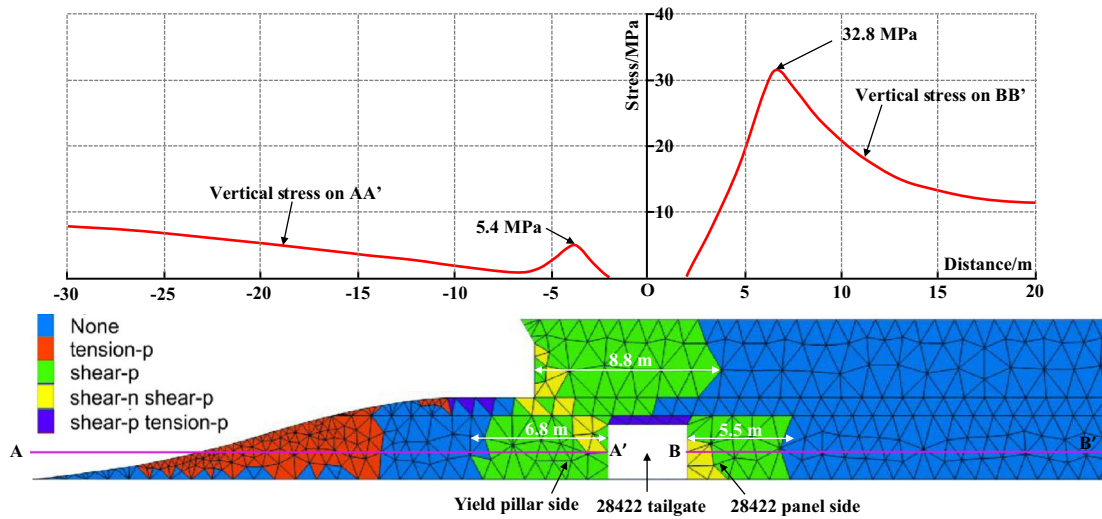
why the roof-to-floor convergence is smaller than rib-to-rib convergence. Most surprisingly, the intact zone in the curved part of the yield pillar (blue elements) is observed, this part may also contribute to the overall stability of the gate pillar. In fact, this unexpected phenomenon has been found and utilized in many coal mining engineering projects in China, and the gate roads are excavated within this intact zone where the stress is far lower than pre-mining stress as we can see from the corresponding locations of the intact zone and the stress distribution in Fig. 10. This layout is being employed by many coal mines in China and ground control problems such as coal bursts, roadway deformation, etc., are minimized (Wang et al. 2017a, b; Zhao et al. 2017). Therefore, stability of gate road can be improved by adjusting gate road layout or conceive innovative pillar designs.

## 5 Field Measurements

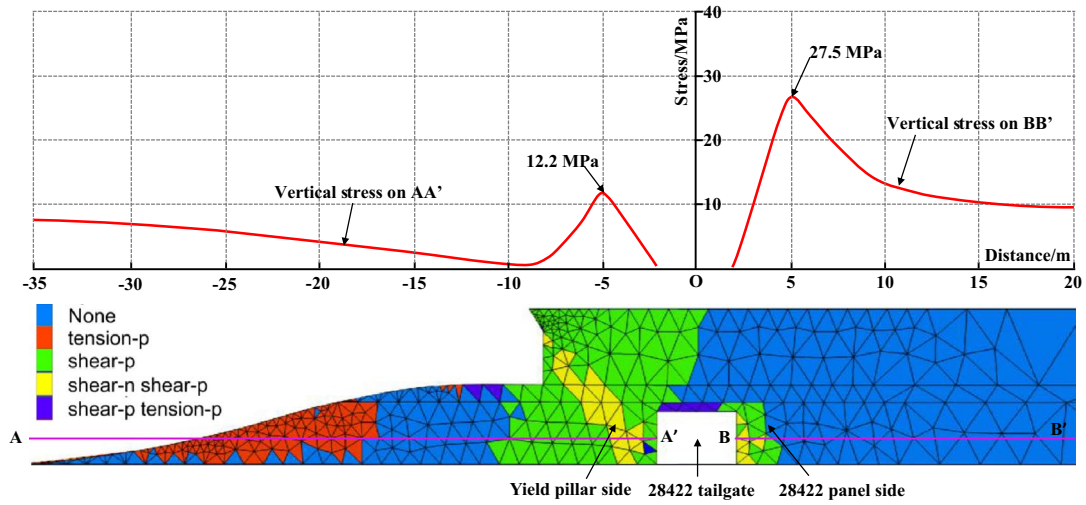
Field measurements were carried out to study the stress distribution within pillar and the convergence law of the gateroad next to the pillar, as well as to validate the numerical modelling.

### 5.1 Pillar Stress Measurements

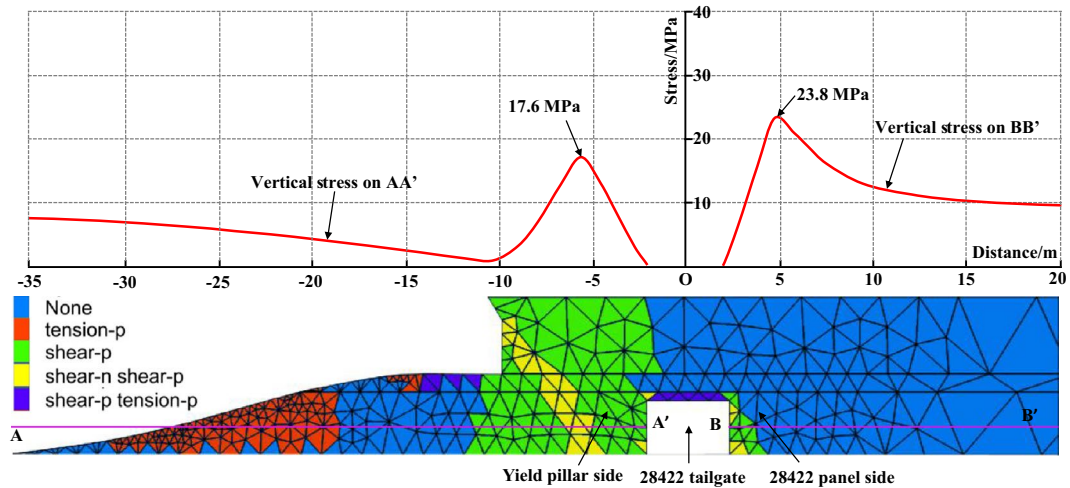
Five stress meters spaced at 50 m apart were installed prior to mining the 28,422 panel at depth of 1, 2, 3, 4 and 5 m into the yield pillar from the tailgate of panel 28,422 to collect stress data. The depth denotes the distance from the rib wall of the 28,422 tailgate into the coal pillar. The instrumentation plan is shown in Fig. 12. The stressmeters were connected to computers, through a data interface. Data were collected and processed every 20 min. These instruments



(a) 4 m yield pillar



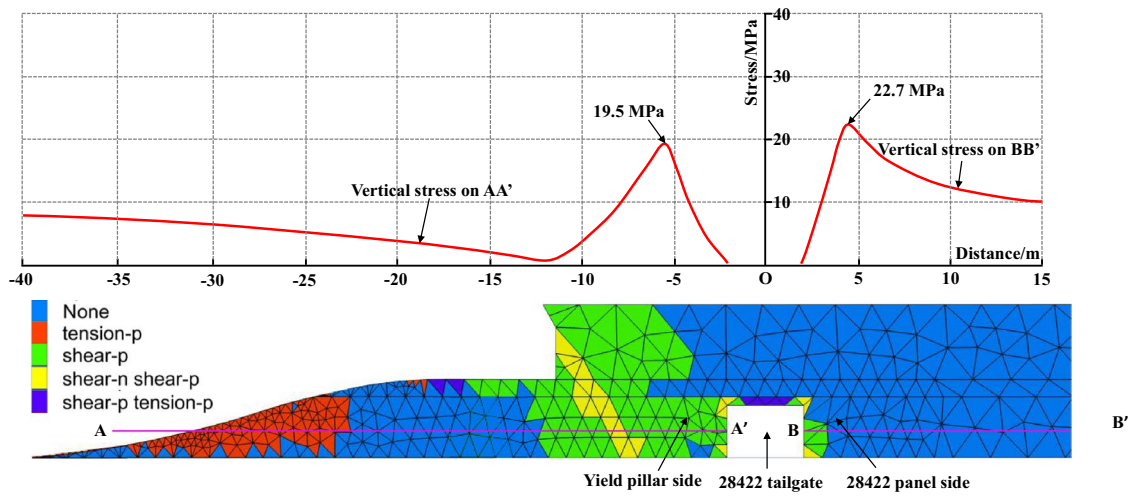
(b) 6 m yield pillar



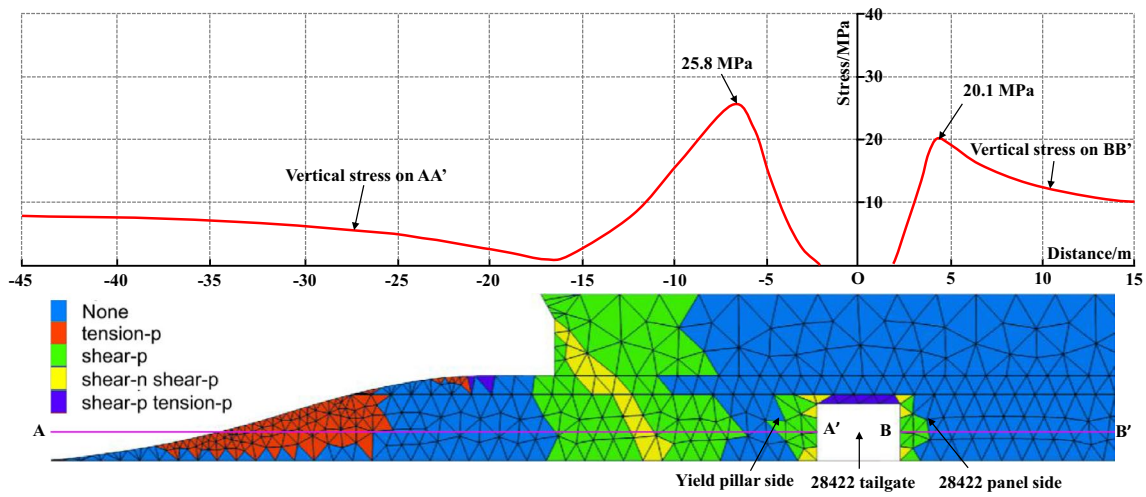
(c) 8 m yield pillar

Fig. 10 Modelling results

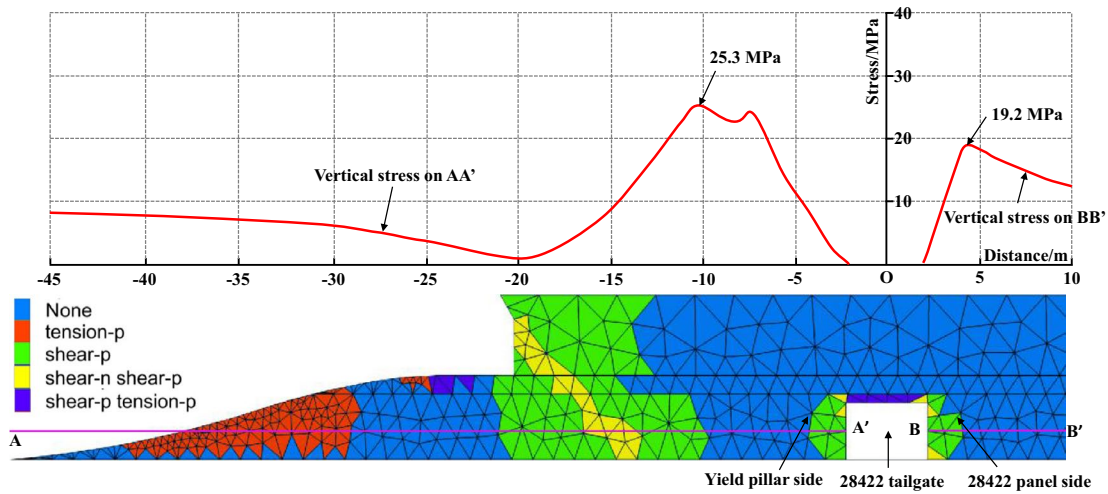




(d) 10 m yield pillar



(e) 14 m yield pillar



(f) 18 m yield pillar

Fig. 10 (continued)

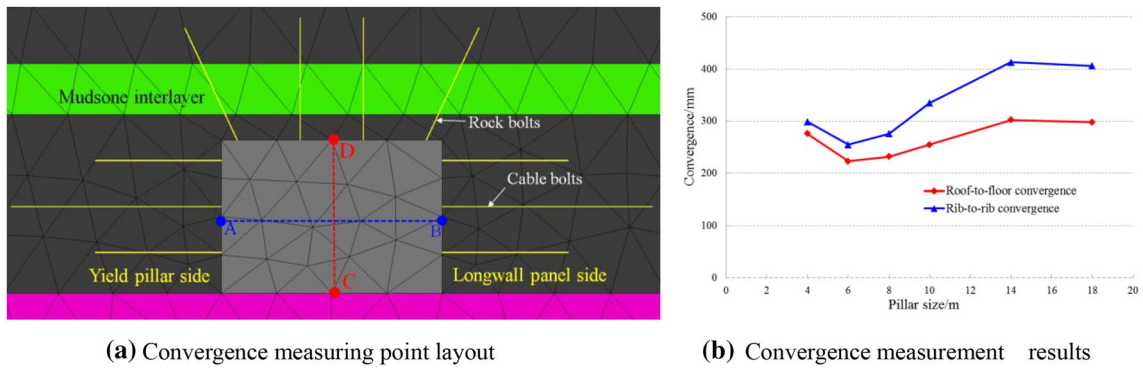
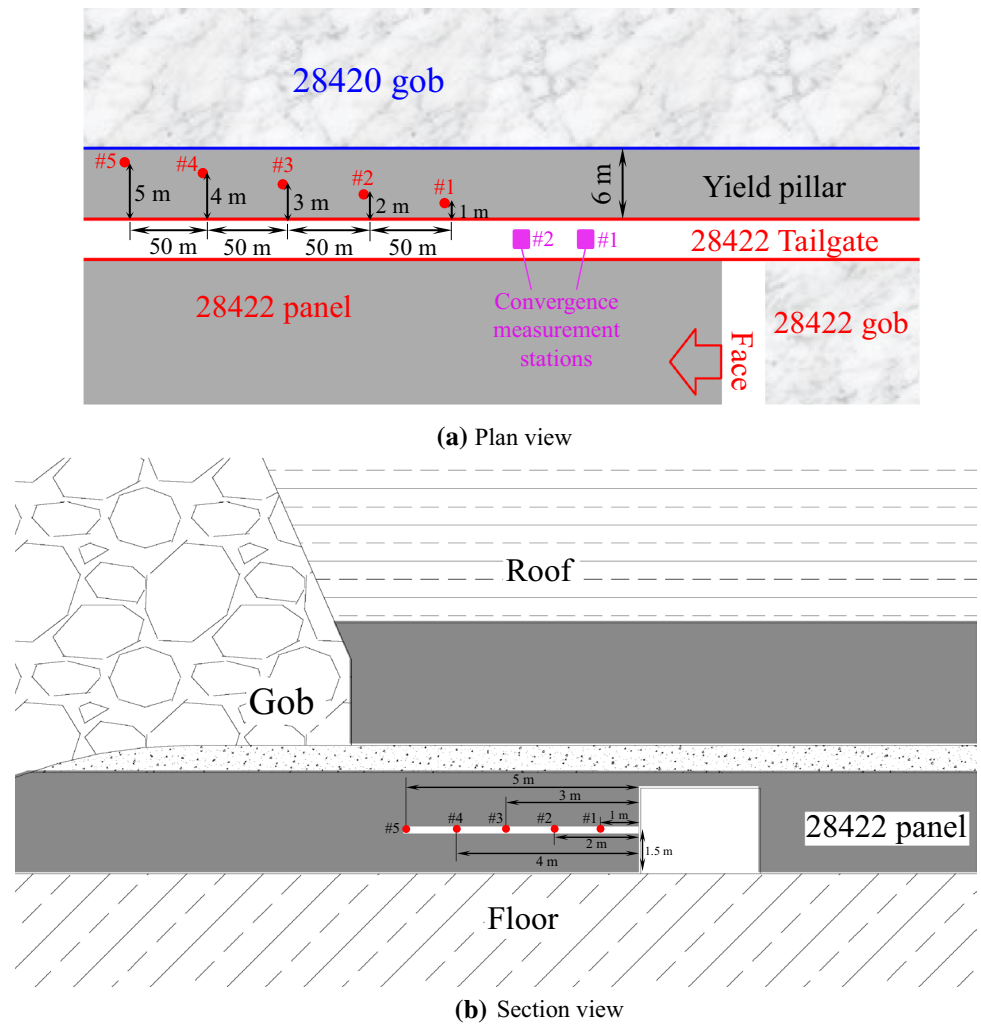


Fig. 11 Convergence measuring points layout and results

Fig. 12 Instrumentation plan of stress meters (localized enlarged views, not to scale)



provided a measure of the vertical stress change with the working face advancement.

### 5.2 Convergence Measurements

Two measurement stations, purple solid squares shown in Fig. 12a, spaced at 50 m were installed immediately after the development of the tailgate of 28,422 panel when headings

was about 600 m away from the main gate. These measurements were to capture mining-induced convergence during entry development and panel retreating. During the panel retreating, multiple rows of individual props spaced at 1.2 m were used for advanced support with a range of 0–50 m ahead of the working face. The convergences of the tailgate ahead of working face were monitored using cross measurement method as shown in Fig. 13. Permanent pins were installed in the roof, floor, pillar rib, and longwall panel rib for each measurement station, respectively. Differences of “AB” and “CD” with respect to their initial values represent rib-to-rib convergence and roof-to-floor convergence, respectively. Rib-to-rib convergence “AB” was measured by a flexible tape, and roof-to-floor convergence was measured using a telescoping rod.

### 5.3 Instrumentation Results

The peak stress in each hole was plotted with respect to the distance from the pillar rib of 28,422 tailgate as shown in Fig. 14. The simulated result shown in Fig. 10b is also plotted in the same figure to make a comparison. It shows that the measured results and simulated result agree well which provides a validation of the numerical modelling. The peak stress occurred at the middle of the pillar, or maybe between 2 and 4 m away from the pillar rib of 28,422 tailgate.

The pillar stress for each measuring point with respect to the distance to the longwall face was plotted in Fig. 15. It shows that the 3# stressmeter which is located in the middle of the pillar underwent largest mining-induced stress, followed by 2#, 4#, 1# and 5# in descending order. Most notably, the stress increase from near 0 MPa at the faceline to its peak value at about 40 m ahead of the working face. Instead of exhibiting a regular stress curve for wide coal pillar that the stress increases to the peak abutment and then drops to pre-mining

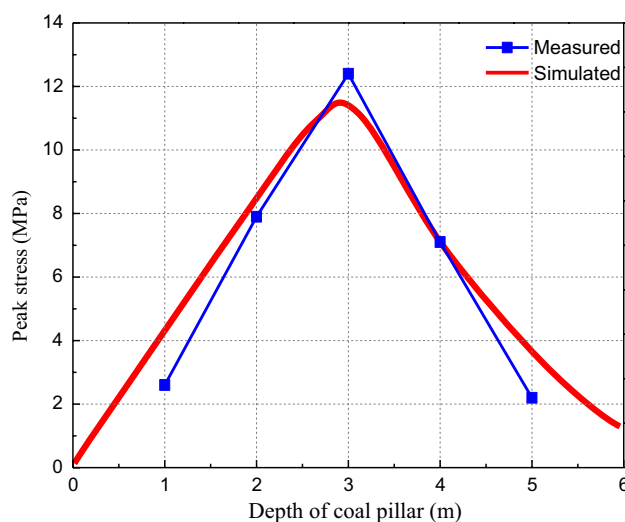


Fig. 14 Vertical stress distribution at each stressmeter across the pillar before retreating of 28,422 panel

stress, stresses distributed in yield pillar in Fig. 15 show that stress increases to peak value without evident dropping to pre-mining stress. This demonstrates that a portion of the pillar close to the working face may experience severe damage, indicating that support capacity may be lost due to repeated loading and unloading during the longwall face advance. And then load bearing capacity of the pillar gradually picked up with the increase of the distance ahead of the working face. The original load bearing capacity of the pillar is achieved at about 40 m away from the working face. According to our published Chinese papers and some unpublished research results, the stress that cannot be sustained by the yield pillar is transferred to the gob of the previous panel, gob behind the working face and solid coal ahead of the working face. Most interestingly, the gob behind the working face at the elevating section bears

Change Collector to Data Collection, Adapter to InterfaceCha

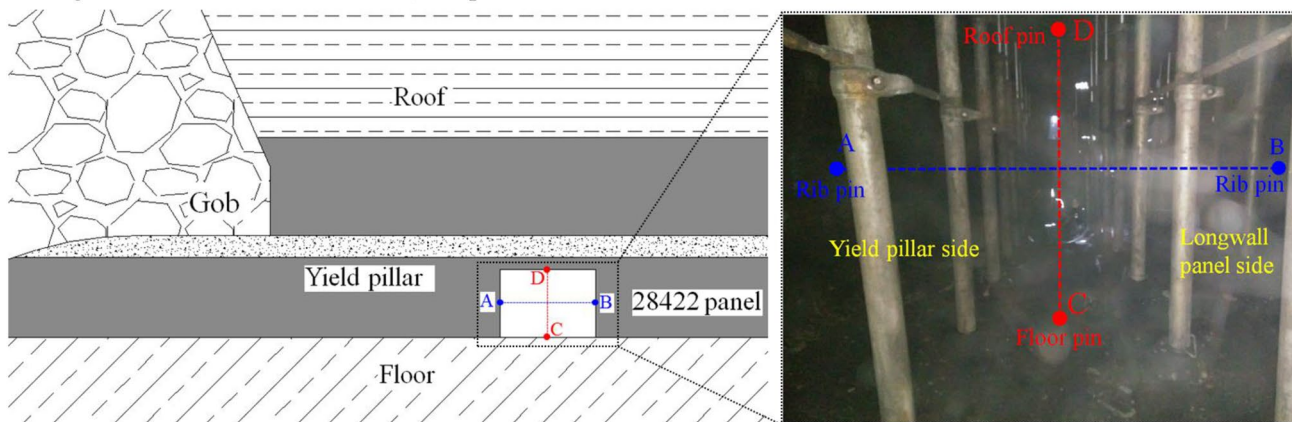
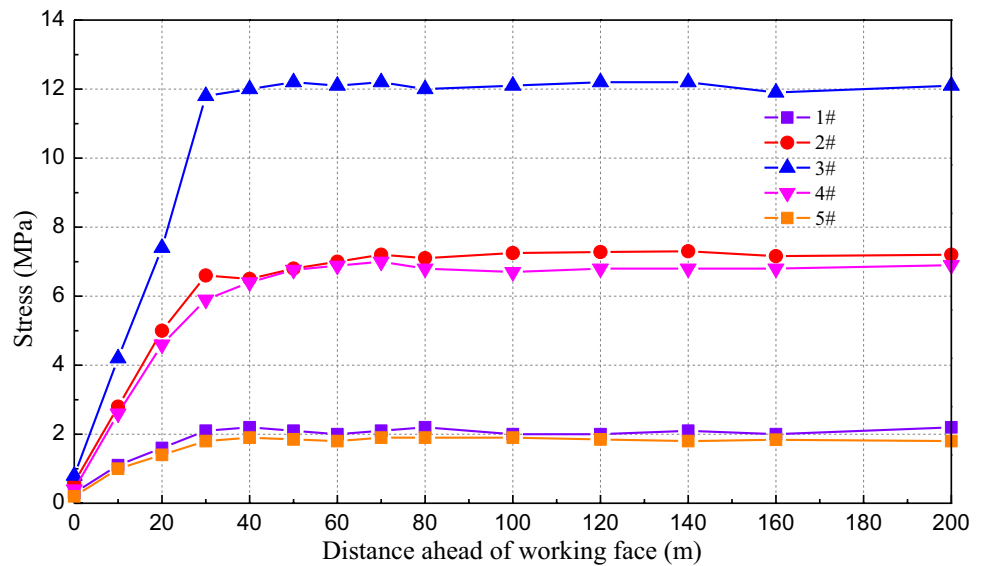


Fig. 13 Schematic of convergence monitoring layout ahead of working face

**Fig. 15** Stress distribution at each stressmeter along the pillar before retreating of 28,422 panel



more load than the other side without this section as the mining height is reduced as shown in Fig. 2b, c.

Figure 16 shows field measurement of convergence of 28,420 and 28,422 tailgates during the development and panel retreat. Simulated convergence of 28,422 tailgate with respect to time step are also plotted in the same figure. It shows that during the development, convergence of 28,422 tailgate next to the yield pillar were smaller than that of 28,420 tailgate. About 95% of the entry convergence occurred within 50 days after entry development. Convergence hardly changed 80 days after development. The maximum roof-to-floor and rib-to-rib convergences of 28,420 tailgate were 375 and 429 mm, respectively, while that of 28,422 tailgate were 235 and 261 mm, respectively. This demonstrates that the roof-to-floor convergence is smaller than rib-to-rib convergence due to the influence of the mudstone interlayer. The field data of convergences of 28,422 tailgate has a good agreement with the simulated results, which also provides a validation for numerical modelling.

During the panel retreat, most of the entry convergence occurred within a range of 40 m ahead of the working face. The maximum convergence values are located at entrance of the tailgates. The maximum roof-to-floor and rib-to-rib convergences of 28,420 tailgate were 1452 and 1527 mm, respectively, while that of 28,422 tailgate were 529 and 551 mm, respectively. This demonstrates that the stability of the tailgate next to the 6-m SPL yield pillar was effectively maintained with reduction of other ground control problems.

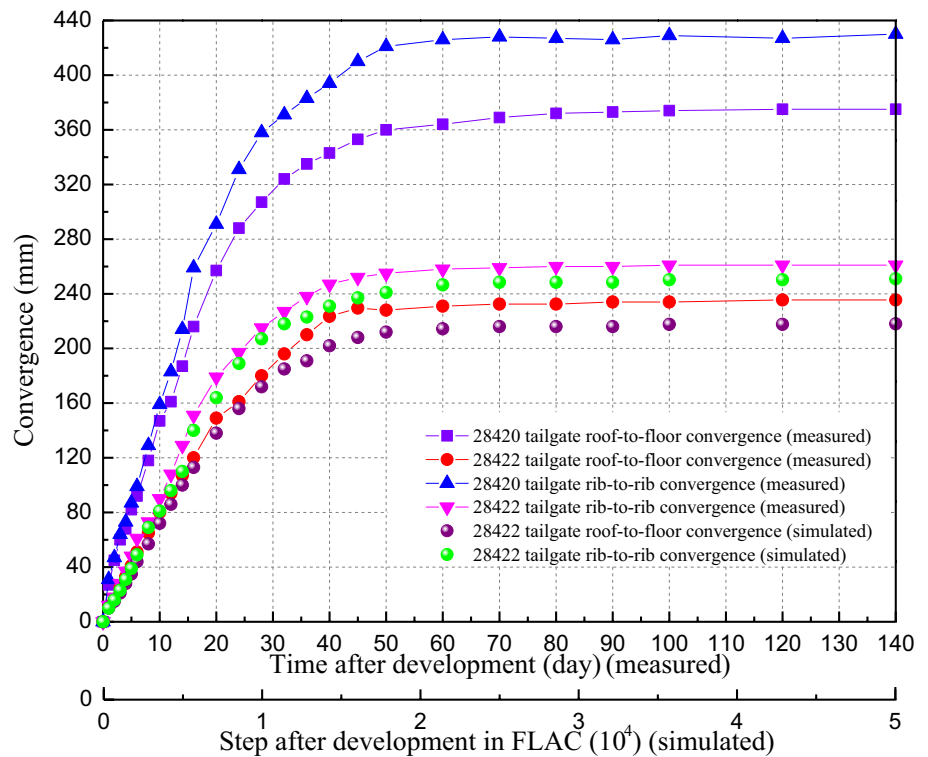
## 6 Conclusions

This paper presents performance of an irregular pillar (non-rectangular and non-square) involving yield pillar application for gate road stability by employing split-level panel layout (SPL) at a coal mine. SPL is being employed to create a better cavability for top coal. Gate roads on either end of a SPL panel are located at different elevations within the 8# and 9# coal seams. The tailgate is driven along the floor of 9# coal seam while the headgate is driven along the roof of 8# coal seam. Thus, the mining geometry consists of a gradually elevating section on one end of the panel. Therefore, the gate pillar is of irregular shape and consists of two coal seams and a mudstone interlayer sandwiched in between. Since theoretical or empirical analysis is very difficult to implement and results may not be valuable or reliable, stability of the tailgate next to this type of irregular yield pillar was investigated through numerical modelling which was then validated by field measurements.

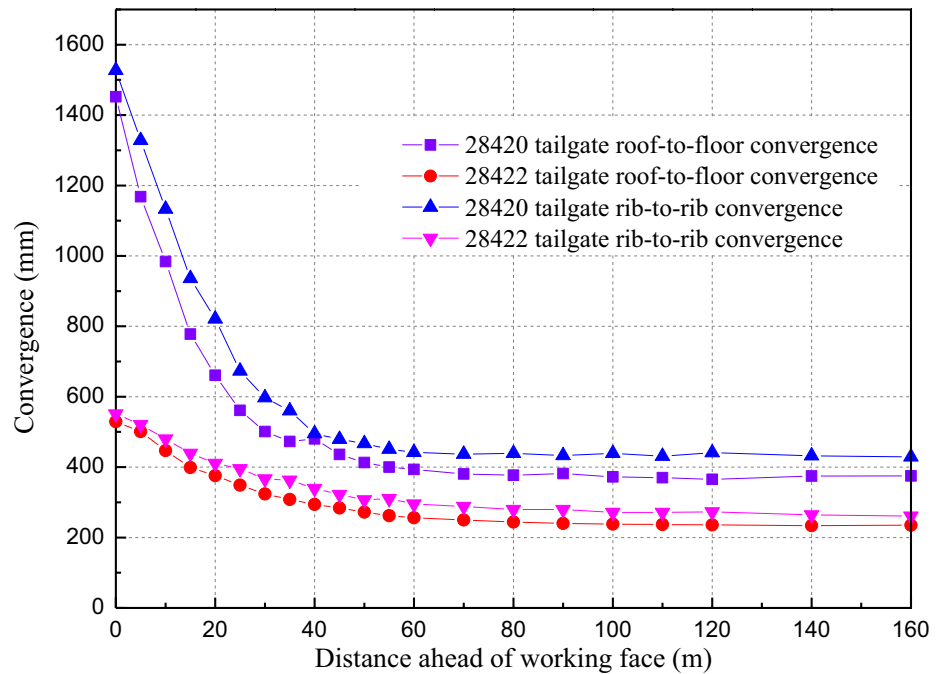
A simple  $FLAC^{3D}$  model was developed that included bedding planes capable of yielding and separating. Bolts were simulated. Mohr–Coulomb constitutive model was used for the rock strata, strain-softening model (a cohesion and internal friction angle loss process) for the yield pillar and double-yield model for the gob. Six yield pillar widths were simulated in the model, i.e., 4, 6, 8, 10, 14



**Fig. 16** Field measurement of convergences of 28,420 and 28,422 tailgates. **a** convergences of 28,420 and 28,422 tailgate against time after development. **b** convergences of 28,420 and 28,422 tailgate against distance ahead of working face



(a) Convergences of 28420 and 28422 tailgate against time after development.



(b) Convergences of 28420 and 28422 tailgate against distance ahead of working face

and 18 m. The results show that tailgate with a 6-m-wide pillar has the minimum deformation. Load-bearing capacity of the pillar and gate road deformation vary with pillar widths which has a considerable effect on stability of the gate road next to the pillar. The mudstone interlayer has

a significant influence on overall stability of tailgate and the yield pillar. The yield zone development and connection of the 8# and 9# coal seams was cut off by this more competent interlayer, the yield zone is smaller especially for the roof of the tailgate which provides a better support

condition for the tailgate. The roof-to-floor convergence is smaller than rib-to-rib convergence. The intact zone in the curved part of the yield pillar (blue elements) is observed that may be contributing to the overall stability of the gate pillar.

The peak stress occurs at the center of the 6-m wide pillar, or about 2–4 m away from the pillar rib of 28,422 tailgate. The center part of the pillar experienced largest mining-induced stress. The yield pillar stress increased to peak value without dropping to pre-mining stress. Thus, a portion of the pillar close to the working face may experience severe damage due to repeated loading and unloading during the longwall face advance. Loading on the pillars gradually increased with the increase in distance ahead of the working face. The original load distribution on the pillar is achieved at about 40 m away from the working face.

Convergence monitoring suggests that during the development convergences of 28,422 tailgate next to the yield pillar were smaller than that of 28,420 tailgate. About 95% of the entry convergence occurred within 50 days after entry development. Convergence became stable 80 days after development. The roof-to-floor convergence is smaller than rib-to-rib convergence due to the influence of the mudstone interlayer. During the panel retreat, most of the entry convergences occurred within a range of 40 m ahead of the working face. The maximum convergence was located at the entrance of the tailgates. Stability of the tailgate next to the 6-m SPL yield pillar was effectively maintained with reduction of other ground control problems.

**Acknowledgements** Special thanks to Y. P. Chugh, Professor Emeritus and visiting professor at Southern Illinois University Carbondale, who performed significant review and editing of the manuscript. The authors are thankful to the anonymous reviewers for their kind suggestions.

**Funding** This study was funded by the National Natural Science Foundation of China, Excellent Young Scientists Fund (no. 51422404); NSFC-Shanxi Joint Fund for Coal-Based Low-Carbon Technology (no. U1710258) and Fundamental Research Funds for the Central Universities (Grant number 2011YZ10).

## Compliance with ethical standards

**Conflict of interest** The authors declare no conflict of interest.

## References

- Agapito JFT, Goodrich TT, Moon M (1997) Dealing with coal bursts at Deer Creek. *Min Eng* 49(7):31–37
- Alejano LR, RamíRez-Oyanguren P, Taboada J (1999) Fdm predictive methodology for subsidence due to flat and inclined coal seam mining. *Int J Rock Mech Min Sci* 36(4):475–491
- Bai QS, Tu SH, Wang FT, Zhang XG, Tu HS, Yuan Y (2014) Observation and numerical analysis of the scope of fractured zones around gate roads under longwall influence. *Rock Mech Rock Eng* 47(5):1939–1950
- Barron K (1984) An analytical approach to the design of coal pillars. *Can Inst Min Bull* 77:37–44
- Brady BHG, Brown ET (2006) *Rock mechanics for underground mining*, 3rd edn. Springer, The Netherlands
- Brauner G (1994) *Rockbursts in coal mines and their prevention*. A.A. Balkema, Amsterdam, p 144
- Cao AY, Dou LM, Wang CB, Yao XX, Dong JY, Gu Y (2016) Microseismic precursory characteristics of rock burst hazard in mining areas near a large residual coal pillar: a case study from Xuzhuang coal mine, Xuzhou, China. *Rock Mech Rock Eng* 49(11):1–16
- Chen Y, Ma SQ, Yu Y (2017) Stability control of underground roadways subjected to stresses caused by extraction of a 10-m-thick coal seam: a case study. *Rock Mech Rock Eng* 50(9):2511–2520
- Colwell M (1998) Chain pillar design—calibration of ALPS. Final report Australian Coal Association Research Program Project C6036
- Corkum AG, Board MP (2016) Numerical analysis of longwall mining layout for a Wyoming trona mine. *Int J Rock Mech Min Sci* 89:94–108
- DeMarco MJ, Koehler JR, Maleki H (1995) Gate road design considerations for mitigation of coal bumps in western U.S. longwall operations. In: Maleki H, Wopat PF, Repsher RC, Tuchman RJ (eds) *Proceedings: mechanics and mitigation of violent failure in coal and hard-rock mines*. U.S. Department of the Interior, Bureau of Mines, SP 01-95, Spokane, WA, NTIS No. PB95211967, pp 141–165.
- Esterhuizen E, Mark C, Murphy M (2010) Numerical model calibration for simulation coal pillars, gob and overburden response. In: *Proceedings of the 29th international conference on ground control in mining*, Morgantown, WV, pp 46–57
- Gales WJ (1998) Coal pillar design issues in longwall mining, in Aziz, N (ed) *Coal 1998: Coal operators' conference*, University of Wollongong and the Australasian Institute of Mining and Metallurgy, pp 133–146
- Gao FQ, Stead D, Kang HP (2015) Numerical simulation of squeezing failure in a coal mine roadway due to mining-induced stresses. *Rock Mech Rock Eng* 48(4):1635–1645
- Ghasemi E, Shahriar K (2012) A new coal pillars design method in order to enhance safety of the retreat mining in room and pillarmines. *Saf Sci* 50:579–585
- Han J, Zhang H, Liang B, Rong H, Lan TW, Liu YZ, Ren T (2016) Influence of large syncline on in situ stress field: a case study of the Kaiping coalfield, China. *Rock Mech Rock Eng* 49(11):23–40
- Hustrulid WA (1976) A review of coal pillar strength formulas. *Rock Mech* 8:115–145
- Itasca (2007) *Fast Lagrangian analysis of continua in 3 dimension, Version 3.1, user's guide*. Itasca Consulting Group Inc., Minneapolis, MN, USA
- Jaiswal A, Shrivastva BK (2009) Numerical simulation of coal pillar strength. *Int J Rock Mech Min Sci* 46(4):779–788
- Jiang YD, Wang HW, Xue S, Zhao YX, Zhu J, Pang XF (2012) Assessment and mitigation of coal bump risk during extraction of an island longwall panel. *Int J Coal Geol* 95:20–33
- Jiang L, Zhang P, Chen L, Hao Z, Sainoki A, Mitri HS (2017) Numerical approach for goaf-side entry layout and yield pillar design in fractured ground conditions. *Rock Mech Rock Eng* 50:3049–3071
- Kang H, Zhang X, Si L, Wu Y, Gao F (2010) In-situ stress measurements and stress distribution characteristics in underground coal mines in China. *Eng Geol* 116: 333–345
- Khair AW (1968) Effect of coefficient of friction on the compressive strength of model coal pillars. MS thesis, West Virginia University, p 101
- King HJ, Whittaker BN (1971) A review of current knowledge on roadway behaviour, especially the problems on which further

- information is required. In: Proceedings of the symposium on strata control in roadway. IME, London, pp 73–90
- Li W, Bai J, Peng S, Wang X, Xu Y (2015) Numerical modeling for yield pillar design: a case study. *Rock Mech Rock Eng* 48(1):305–318
- Li ZL, Dou LM, Cai W, Wang GF, Ding YL, Kong Y (2016a) Roadway stagger layout for effective control of gob-side rock bursts in the longwall mining of a thick coal seam. *Rock Mech Rock Eng* 49(2):621–629
- Li HM, Peng S, Li HG, Xu YX, Yuan RF, Yue SS, Li K (2016b) Trial of small gate road pillar in top coal caving longwall mining of large mining height. *Int J Min Sci Technol* 26(1):139–147
- Madden BJ (1991) A re-assessment of coal-pillar design. *J S Afr IMin Metall* 91:27–37
- Maleki H (2017) Coal pillar mechanics of violent failure in U.S. Mines. *Int J Min Sci Technol* 27(3):387–392
- Mark C (1990) Pillar design methods for longwall mining. Bureau of Mines, Pittsburgh, p 53
- Mark C (2016) Coal bursts in the deep longwall mines of the United States. *Int J Coal Sci Technol* 3(1):1–9
- Mark C, Gale W, Oyler D, Chen J (2007) Case history of the response of a longwall entry subjected to concentrated horizontal stress. *Int J Rock Mech Min Sci* 44(2):210–221
- Medhurst TP, Brown ET (1998) A study of the mechanical behaviour of coal for pillar design. *Int J Rock Mech Min Sci* 35(8):1087–1105
- Meikle PG (1965) Effect of friction on the strength of model coal pillars. M.S. thesis, West Virginia University, p 61
- Mohan GM, Sheorey PR, Kushwaha A (2001) Numerical estimation of pillar strength in coal mines. *Int J Rock Mech Min Sci* 38(8):1185–1192
- Morsy K, Peng SS (2002) Numerical modeling of the gob loading mechanism in longwall coal mines. In: Proceedings of the 21st international conference on ground control in mining, Morgantown, WV, pp 58–67
- Mortazavi A, Hassani FP, Shabani M (2009) A numerical investigation of rock pillar failure mechanism in underground openings. *Comput Geotech* 36(5):691–697
- Nazimko VV (1994) Pillarless longwall mining for multiple seams. In: Peng SS (ed) Proceedings of the 13th international conference, ground control in mining, Morgantown, WV, 1994 (WVU/USBM), pp 239–245
- Newman DA (2002) A case history investigation of two coal bumps in the southern appalachian coalfield. In: Proceedings of the 21st international conference on ground control in mining. West Virginia University, Morgantown, WV, pp 90–97
- Pappas DM, Mark C (1993) Behavior of simulated longwall gob material. US Department of the Interior, Bureau of Mines, Pittsburgh
- Peng SS (2006) Longwall mining, 2nd edn. Peng SS Publisher, Morgantown
- Peng SS (2008) Coal mine ground control, 3rd edn. Peng SS publisher, Morgantown, pp 229–237 (359–363, 422–423)
- Recio-Gordo D, Jimenez R (2012) A probabilistic extension to the empirical ALPS and ARMPS systems for coal pillar design. *Int J Rock Mech Min Sci* 52:181–187
- RocData. Available online: <https://www.rocsience.com/rocsience/products/rocddata>. Accessed 10 Oct 2016
- Salamon MDG (1990) Mechanism of caving in longwall coal mining MDG Salamon. In: Rock mechanics contributions and challenges: Proceedings of the 31st US symposium on rock mechanics
- Salamon MDG, Munro AH (1967) A study of the strength of coalpillars. *J S Afr I Min Metall* 68:55–67
- Seedsman R, Jalafar H, Aziz N (2005) Chain pillar design—can we?. In: Aziz N (ed) Coal 2005: coal operators' conference. University of Wollongong and the Australasian Institute of Mining and Metallurgy, pp 59–62
- Shabanimashcool M, Li CC (2012) Numerical modeling of longwall mining and stability analysis of the gates in a coal mine. *Int J Rock Mech Min Sci* 51:24–34
- Shabanimashcool M, Li CC (2013) A numerical study of stress changes in barrier pillars and a border area in a longwall coal mine. *Int J Coal Geol* 106:39–47
- Shen B (2014) Coal mine roadway stability in soft rock: a case study. *Rock Mech Rock Eng* 47:2225–2238
- Smart BGD, Haley SM (1987) Further development of the roof strata. *Min Sci Technol* 5:121–130
- Singh AK, Singh R, Maiti J, Mandal PK (2011) Assessment of mining induced stress development over coal pillars during depillaring. *Int J Rock Mech Min Sci* 48(5):805–818
- Song GF, Chugh YP, Wang JC (2017) A numerical modelling study of longwall face stability in mining thick coal seams in China. *Int J Min Miner Eng* 8(1):35–55
- Tan YL, Yu FH, Ning JG, Zhao TB (2015) Design and construction of entry retaining wall along a gob side under hard roof stratum. *Int J Rock Mech Min Sci* 77:115–121
- Wang SY, Sloan SW, Huang ML, Tang CA (2011) Numerical study of failure mechanism of serial and parallel rock pillars. *Rock Mech Rock Eng* 44:179–198
- Wang HW, Jiang Yd, Zhao YX, Zhu J, Liu S (2013) Numerical investigation of the dynamic mechanical state of a coal pillar during longwall mining panel extraction. *Rock Mech Rock Eng* 46(5):1211–1221
- Wang HW, Jiang YD, Xue S, Pang XF, Lin AN, Deng DX (2016) Investigation of intrinsic and external factors contributing to the occurrence of coal bumps in the mining area of Western Beijing, China. *Rock Mech Rock Eng* 50(4):33–47
- Wang JC, Wang ZH, Yang SL (2017a) A coupled macro- and meso-mechanical model for heterogeneous coal. *Int J Rock Mech Min Sci* 94:64–81
- Wang PF, Zhao JL, Chugh YP, Wang ZQ (2017b) A novel longwall layout approach for extraction of deep inclined coal deposits. *Minerals* 7(4):60
- Wilson AH (1972) An hypothesis concerning pillar stability. *Min Eng (Lond)* 131:409–417
- Wilson AH (1981) Stress and stability in coal ribsides and pillars. In: Proceedings of the first international conference on ground control in mining. West Virginia University, Morgantown, WV, pp 1–12
- Yan S, Bai J, Wang X, Huo L (2013) An innovative approach for gate road layout in highly gassy longwall top coal caving. *Int J Rock Mech Min Sci* 59:33–41
- Yang H, Cao S, Li Y, Sun C, Guo P (2015) Soft roof failure mechanism and supporting method for gob-side entry retaining. *Minerals* 10:707–722
- Yasitli NE, Unver B (2005) 3D numerical modeling of longwall mining with top-coal caving. *Int J Rock Mech Min Sci* 42:219–235
- Yavuz H (2004) An estimation method for cover pressure re-establishment distance and pressure distribution in the goaf of longwall coal mines. *Int J Rock Mech Min Sci* 41:193–205
- Yu B (2016) Behaviors of overlying strata in extra-thick coal seams using top-coal caving method. *J Rock Mech Geotech Eng* 8:238–247
- Yu B, Zhang Z, Kuang T, Liu J (2016) Stress changes and deformation monitoring of longwall coal pillars located in weak ground. *Rock Mech Rock Eng* 49:3293–3305
- Zhang K, Zhang GM, Hou RB, Wu Y, Zhou HQ (2014) Stress evolution in roadway rock bolts during mining in a fully mechanized longwall face, and an evaluation of rock bolt support design. *Rock Mech Rock Eng* 48:333–344
- Zhang Z, Bai J, Chen Y, Yan S (2015a) An innovative approach for gob-side entry retaining in highly gassy fully-mechanized longwall top-coal caving. *Int J Rock Mech Min Sci* 80:1–11

- Zhang ZZ, Bai JB, Chen Y, Yan S (2015b) An innovative approach for gob-side entry retaining in highly gassy fully-mechanized longwall top-coal caving. *Int J Rock Mech Min Sci* 80:1–11
- Zhang ZT, Zhang R, Xie HP, Gao MZ, Xie J (2016) Mining-induced coal permeability change under different mining layouts. *Rock Mech Rock Eng* 49(9):53–68
- Zhang GC, He FL, Jia HG, Lai YH (2017) Analysis of gate road stability in relation to yield pillar size: a case study. *Rock Mech Rock Eng* 1:1–16
- Zhao JL, Wang PF, Su Y (2017) An innovative longwall mining technology in Tangshan coal mine, China. *Minerals* 7(1):14
- Zhu ST, Feng Y, Jiang FX (2016) Determination of abutment pressure in coal mines with extremely thick alluvium stratum: a typical kind of rockburst mines in China. *Rock Mech Rock Eng* 49(5):1943–1952

**Publisher's Note** Springer Nature remains neutral with regard to jurisdictional claims in published maps and institutional affiliations.